

AGE OF MASSIVE GALAXIES AT REDSHIFT 8

M. LÓPEZ-CORREDOIRA^{1,2,3}, F. MELIA^{4,5}, J.-J. WEI^{6,7}, C.-Y. GAO^{6,7}

Draft version May 24, 2024

ABSTRACT

Recent James Webb Space Telescope (JWST) data analyses have shown that massive red galaxies existed at redshifts $z \gtrsim 6$, a discovery that is difficult to understand in the context of standard cosmology (Λ CDM). Here we analyze these observations more deeply by fitting a stellar population model to the optical and near-infrared photometric data. These fits include a main stellar population in addition to a residual younger population and with the same extinction for both (a lower extinction for the younger population is unphysical). Extra stellar populations or the inclusion of an AGN component do not significantly improve the fits. These galaxies are being viewed at very high redshifts, with an average $\langle z \rangle \approx 8.2$, when the Λ CDM Universe was only ≈ 600 Myr old. This result conflicts with the inferred ages of these galaxies, however, which were on average between 0.9 and 2.4 Gyr old within 95% CL. Given the sequence of star formation and galaxy assembly in the standard model, these galaxies should instead be even younger than 290 Myr on average, for which our analysis assigns a probability of only $< 3 \times 10^{-4}$ ($\gtrsim 3.6\sigma$ tension). This outcome may indicate the need to consider non-standard cosmologies. Nevertheless, our conclusions result from several approximations in stellar astrophysics and extinction, so they should be taken with a grain of salt. Further research is necessary to corroborate the possible existence of galaxies older than the Λ CDM universe at their observed redshifts.

Keywords: Observational cosmology (1146); High-redshift galaxies (734).

1. INTRODUCTION

Recent James Webb Space Telescope (JWST) data analyses have shown that massive red galaxies existed at redshifts $z \gtrsim 6$, a discovery that is difficult to understand in the context of standard cosmology (Λ CDM) (Labbé et al. 2023; Boylan-Kolchin 2023). Here we investigate the age of these galaxies, providing additional evidence of an unavoidable controversy if they are old, as we shall demonstrate in this paper, especially if they are older than the presumed age of the Universe at the time corresponding to their redshifts.

There is a broad literature on the topic of the old age of massive high- z galaxies, and the tension this produces for standard theories of galaxy formation (López-Corredoira 2022, Sect. 7.2). Recent JWST observations have discovered very high redshift galaxies, up to 17, with derived estimates of some of their ages (Melia 2023). The high density of these galaxies has been called the ‘impossibly

early galaxy’ problem, based on the detection of several orders of magnitude more massive haloes at very much higher redshift than predicted (Steinhardt et al. 2016). Furthermore, the large rotational velocity and large content of cold gas in some high redshift galaxies remain a challenge to efforts of reproducing the standard predictions of galaxy formation (Neeleman et al. 2020).

The usual methods for determining the galaxies’ age include SED (Spectral Energy Distribution) fitting or spectral analyses. Spectral analyses may provide more accurate measurements, but require very large exposure times, so they are available only for a few galaxies and are importantly affected by the age-metallicity degeneracy in those cases of low signal/noise (Cardiel et al. 2003). Nonetheless, there have been some useful studies in this direction. For instance, Schiavon et al. (2006) used the strength of H_δ for $z \sim 0.9$ galaxies and the fit of the whole spectrum in their models. Their approach seems also appropriate for our galaxies with redshift up to 1.2. A more accurate method of age determination, such as the use of H_γ (Vazdekis & Arimoto 1999; Yamada et al. 2006), would need a very high signal/noise in the spectra, which is not reachable for high redshift galaxies. However, Glazebrook et al. (2017); Schreiber et al. (2018) were able to analyze the spectra of quiescent galaxies from the FourStar Galaxy Evolution Survey (ZFOURGE) using the combined $H_\beta + H_\gamma + H_\delta$ absorption lines at $3 < z < 4$ to infer stellar ages $\lesssim 1$ Gyr. Another possible age determination is given through some break. Spinrad et al. (1997) used the breaks at 2640 Å and 2900 Å and the fit of the whole spectrum to deter-

¹ Instituto de Astrofísica de Canarias, E-38205 La Laguna, Tenerife, Spain; martin@lopez-corredoira.com

² PIFI-Visiting Scientist 2023 of Chinese Academy of Sciences at PMO⁶ and National Astronomical Observatories, Beijing 100012, China

³ Departamento de Astrofísica, Universidad de La Laguna, E-38206 La Laguna, Tenerife, Spain

⁴ Department of Physics, The Applied Math Program, and Department of Astronomy, The University of Arizona, AZ 85721, USA

⁵ John Woodruff Simpson Fellow

⁶ Purple Mountain Observatory, Chinese Academy of Sciences, Nanjing 210023, China

⁷ School of Astronomy and Space Sciences, University of Science and Technology of China, Hefei 230026, China

mine that the age of a galaxy at $z = 1.55$ was larger than 3.5 Gyr. Balmer break has been used in JWST high- z galaxies with different results (Steinhardt et al. 2023; Vikaeus et al. 2024). But the Balmer break alone cannot break the dust-age degeneracy, so a more global analysis of the spectral energy distribution is required.

By pushing our observations to redshifts larger than six, we are contributing here to an exploration of this long-standing and deepening crisis that has thus far eluded any clear resolution. In this paper, we shall use the technique of SED fitting because, for the available spectra of JWST high z galaxies (e.g., Schaerer et al. 2022; Curtis-Lake et al. 2023; Vikaeus et al. 2024), the resolution and signal/noise of absorption lines are not enough to permit a determination of their ages. In particular, for the 13 galaxies selected by Labbé et al. (2023), there are only four of them with spectra (see Table 1) with significant signal/noise only for some emission lines, thus they do not permit the analysis of absorption lines or breaks in the continuum.

2. DATA

With the first observations by the JWST Cosmic Evolution Early Release Science (CEERS) program, multi-band photometry at 1-5 μ m (filters F115W, F150W, F200W, F277W, F356W, F410M, F444W), together with preexisting Hubble Space Telescope (HST) photometry in the visible (filters F435W, F606W, F814N), a catalog of 42 729 sources over an ≈ 38 arcmin² field of view has been produced. Within this catalog, galaxies have been selected based on the criteria that they were not detected in the HST filters [SNR(F435W, F606W, F814N) < 2], but have a double break around the Lyman- α and Balmer spectral regions corresponding to redshifts $7 \lesssim z \lesssim 9$ [F150W-F277W < 0.7; F277W-F444W > 1.0], with good SNR [F444W < 27 AB; F150W < 29 AB; SNR(F444W) > 8]. These criteria were chosen: (i) to ensure no secondary redshift solutions at low- z , and (ii) to filter massive galaxies with high M/L ratios. A manual inspection ensured the absence of any artefacts in the images. In total, a subsample of 13 galaxies was obtained by Labbé et al. (2023), the data we shall use throughout this paper.

The conversion of F_ν into F_λ considers the shape of the transmission curves, $T(\lambda)$, of the filters: $F_\lambda(\text{erg s}^{-1} \text{cm}^{-2} \text{\AA}^{-1}) = 2.998 \times 10^{-14} F_\nu(nJy) \times \frac{\Delta\nu}{\Delta\lambda}$, $\Delta\lambda = \frac{[\int d\lambda T(\lambda)]^2}{\int d\lambda T^2(\lambda)}$ $\Delta\nu = \frac{[\int d\nu T(\nu)]^2}{\int d\nu T^2(\nu)}$.

Four of these galaxies have spectroscopic redshifts. For the remaining nine, we calculate photometric redshifts that are quite reliable: spectroscopic and photometric redshifts agree within the error bars and there is a very low probability of including interlopers in the catalog (Finkelstein et al. 2023), as confirmed for the four galaxies with spectroscopic redshifts in our sample (Kocevski et al. 2023; Fujimoto et al. 2023).

3. SED FITTING WITH TWO SSPS

3.1. Method

When we plot the SED of these 13 sources using F_λ vs. λ instead of F_ν vs. λ , we clearly see the characteristic V-shape of a double-aged population in every case (Fig. 1). Note that the x -axis represents the rest wavelength, i.e.,

$\lambda_{\text{observed}}/(1+z)$, where z is derived via the fitting described below, but this conversion of the spectrum into the rest frame does not affect its shape. An alternative selection of JWST high- z galaxies within the catalog of extremely red objects (EROs) is also dominated by V-shaped SEDs (Barro et al. 2024): JWST-CEERS EROs show blue color in the short-wavelength NIRCcam bands (F150W - F277W ~ 0), even without requiring a priori any constraint around the Lyman-break.

We cannot explain these SEDs with a single stellar population (SSP), either young or old. The fact that there exists a valley between the two high peaks around the Lyman- α and Balmer breaks, with a minimum at $\lambda_{\text{rest}} \sim 3000 \text{\AA}$, indicates that we need at least two SSPs to model the photometry (López-Corredoira et al. 2017; Gao et al. 2024): a young one (very luminous at far-UV, but with a very low stellar mass contribution: < 5% in the sample of López-Corredoira et al. (2017); and we will see in §3.2/Table 2 that the best fits give ratios $\leq 1\%$, though with wide errors, for 12 of 13 galaxies treated here) to account for the first peak, and an older one to explain the second. A single SSP of ~ 100 Myr may produce a double peak too, but with very low amplitude, which is not enough to reproduce the conspicuous V-shape we observe. Exponentially decaying, extended star formation models improve the fits slightly with respect to just one SSP model, but they are considerably worse than fits with two SSPs, further supporting the residual star formation scenario (López-Corredoira et al. 2017). In Appendix C, we corroborate this result with the present sample. This remaining contribution from a young, likely residual, star formation component with an age ≤ 100 Myr, is consistent with an in situ formation scenario, likely produced by a more recent episode of gas accretion.

The galaxies we model show this V-shaped SED profile, and are massive and red with no indication of a large extinction (otherwise we would not see the far-UV component), typical of relatively old quiescent component-dominated structures; as we shall see, they are well described, on average, by two SSPs. In our analysis, one of the SSPs is relatively old, while the second is young. We fit the free parameters by minimizing the reduced chi-square. In total, we use six free parameters, aside from the amplitude. These are: the redshift (z , assumed to be ≥ 5 ; spectroscopic when available and fitted otherwise), the ratio of old/young population (A_2), the age of the old population (age_{old}), the age of the young population ($\text{age}_{\text{young}}$), the metallicity [M/H] (the same for both populations; indeed, it is not important what the metallicity is for the younger component because the models are almost completely insensitive to it), and the internal extinction in the V-filter at rest (A_V ; assumed to be ≤ 3.0). The age-metallicity-dust degeneracy (Conroy 2013) may appear when we have little information on the photometry, for instance some few colors; in the selected filters, however, we are able to break this degeneracy. In particular, the Balmer break is affected very little by the extinction and is mostly dependent on age, with some small dependence on metallicity. In any case, the error bars of our fits indicate the level of this degeneracy. The fit of the data using a model with f free parameters (in our case here, $f = 7$) is carried out with a conventional

Table 1

Best fit results with two SSPs. Errors represent the limits for which the templates of GALAXEV fit the data within 95% CL ($\equiv 2\sigma$) (within the resolution of the templates). The ages are expressed in Gyr. Redshifts of id. 13050, 28984, 35900, 39575 are fixed to their spectroscopic [S] values (<https://dawn-cph.github.io/dja/spectroscopy/nirspec/>). References for the spectroscopic redshifts: Kocevski et al. (2023): [Koc23]; Fujimoto et al. (2023): [Fuj23].

Galaxy ID	z	$\log_{10}[\text{age}_{\text{old}}]$	$\log_{10}[\text{age}_{\text{young}}]$	A_2	$[M/H]$	A_V	χ^2_{red}
2859	$9.85^{+0.87}_{-0.50}$	$0.40^{+0.64}_{-0.59}$	$-2.30^{+1.30}_{-0}$	$0.02^{+0.05}_{-0.01}$	$+0.4^{+0}_{-0.8}$	$0^{+1.5}_{-0}$	1.69
7274	$9.87^{+1.33}_{-3.87}$	$0.70^{+0.34}_{-1.24}$	$-2.30^{+1.30}_{-0}$	$0.03^{+0.48}_{-0.02}$	-0.4 ± 0	$0.07^{+1.43}_{-0.07}$	29.39
11184	$7.18^{+0.47}_{-0.39}$	$-0.54^{+0.34}_{-0.46}$	$-1.00^{+0.29}_{-1.30}$	$0.48^{+0.16}_{-0.47}$	$0^{+0}_{-0.4}$	$0^{+0.75}_{-0}$	11.62
13050	5.62 [Koc23]	$1.04^{+0.00}_{-2.64}$	$-2.30^{+3.00}_{-0.00}$	$0.51^{+0.21}_{-0.51}$	$+0.4^{+0}_{-0.8}$	$2.05^{+0.95}_{-2.05}$	7.47
14924	$9.16^{+1.04}_{-0.76}$	$1.04^{+0}_{-1.58}$	$-1.60^{+0.60}_{-0.70}$	$0.12^{+0.24}_{-0.06}$	$+0.4^{+0}_{-0.8}$	$0.31^{+0.79}_{-0.31}$	4.47
16624	$9.83^{+1.97}_{-1.03}$	$1.04^{+0}_{-2.04}$	$-2.30^{+1.30}_{-0}$	$0.09^{+0.27}_{-0.07}$	$+0.4^{+0}_{-0.8}$	$0.45^{+0.55}_{-0.45}$	8.26
21834	$9.87^{+0.56}_{-0.52}$	$1.04^{+0}_{-1.24}$	$-1.60^{+0.60}_{-0.70}$	$0.06^{+0.09}_{-0.03}$	$+0.4^{+0}_{-0.8}$	$0.26^{+0.74}_{-0.26}$	0.39
25666	$6.83^{+3.17}_{-1.83}$	$1.04^{+0}_{-2.64}$	$-1.60^{+2.30}_{-0.70}$	$0.22^{+0.38}_{-0.22}$	$+0.4^{+0}_{-0.8}$	$0.10^{+1.90}_{-0.10}$	24.00
28984	7.09 [S]	$1.04^{+0}_{-1.09}$	$-2.30^{+1.30}_{-0}$	$0.19^{+0.41}_{-0.15}$	$+0.4^{+0}_{-0.8}$	$0.32^{+1.68}_{-0.32}$	4.51
35300	7.77 [Fuj23]	$1.04^{+0}_{-1.24}$	$-2.30^{+1.76}_{-0.00}$	$0.27^{+0.33}_{-0.24}$	$+0.4^{+0}_{-0.8}$	$1.25^{+0.85}_{-1.25}$	1.81
37888	$6.98^{+3.02}_{-1.98}$	$1.04^{+0}_{-2.64}$	$-1.60^{+2.30}_{-0.70}$	$0.70^{+0.29}_{-0.67}$	-0.4 ± 0	$0.51^{+1.49}_{-0.51}$	7.68
38094	$8.10^{+0.62}_{-2.10}$	$-0.54^{+1.58}_{-0.46}$	$-2.30^{+2.11}_{-0}$	$0.02^{+0.58}_{-0.02}$	$0^{+0}_{-0.4}$	$0.42^{+1.58}_{-0.42}$	142.92
39575	7.99 [Fuj23]	$1.04^{+0.00}_{-2.64}$	$-2.30^{+2.26}_{-0}$	$0.62^{+0.24}_{-0.59}$	-0.4 ± 0	$1.49^{+0.61}_{-1.49}$	3.39
Stacked: all	—	$1.04^{+0}_{-0.90}$	$-2.30^{+0.70}_{-0}$	$0.31^{+0.29}_{-0.21}$	$+0.4^{+0}_{-0.8}$	$1.06^{+0.94}_{-1.06}$	6.34
Stacked: 4 z_{spec}	—	$1.04^{+0}_{-0.90}$	$-2.30^{+0.70}_{-0}$	$0.26^{+0.34}_{-0.17}$	$+0.4^{+0}_{-0.8}$	$0.89^{+1.11}_{-0.89}$	4.08
St.a, $\lambda_r \leq 5000\text{\AA}$	—	$1.04^{+0}_{-1.09}$	$-1.60^{+0.40}_{-0.70}$	$0.53^{+0.16}_{-0.25}$	-0.4 ± 0	$0.75^{+0.31}_{-0.75}$	0.56
St.4, $\lambda_r \leq 5000\text{\AA}$	—	$1.04^{+0}_{-1.09}$	$-2.30^{+0.70}_{-0}$	$0.24^{+0.36}_{-0.18}$	$+0.4^{+0}_{-0.8}$	$0.72^{+1.28}_{-0.72}$	4.51
St.a, $\lambda_r \leq 4000\text{\AA}$	—	$1.04^{+0}_{-1.24}$	$-1.60^{+0.40}_{-0.70}$	$0.18^{+0.54}_{-0.04}$	$+0.4^{+0}_{-0.8}$	$0.38^{+0.72}_{-0.26}$	0.37
St.4, $\lambda_r \leq 4000\text{\AA}$	—	$1.04^{+0}_{-2.64}$	$-2.30^{+0.70}_{-0}$	$0.29^{+0.46}_{-0.19}$	$+0.4^{+0}_{-0.8}$	0.75 ± 0.75	1.24

minimization of χ^2 to the theoretical fluxes:

$$F_{\text{theor.}}(\lambda_i) = \frac{L_0}{4\pi d_L(z)^2(1+z)} \times \quad (1)$$

$$\langle [L_{\text{SSP}}(\text{age}_{\text{old}}, [M/H], A_V; \lambda/(1+z))]_T \rangle + A_2 \langle [L_{\text{SSP}}(\text{age}_{\text{young}}, [M/H], A_V; \lambda/(1+z))]_T \rangle,$$

where $\langle (\dots)_T \rangle = \frac{\int d\lambda (\dots)_T(\lambda)}{d\lambda T(\lambda)}$; $d_L(z)$ is the luminosity distance, assuming Λ CDM with $H_0 = 70 \text{ km s}^{-1} \text{ Mpc}^{-1}$ and $\Omega_\Lambda = 0.7$. Note that this conversion of flux into luminosity needs a cosmological model, but the SED fitting is totally independent of the cosmology; d_L affects only the amplitude of the luminosity, not its shape used in the SED fitting.

The theoretical spectra $L_0 L_{\text{SSP}}$ are derived using the GALAXEV stellar population synthesis model (Bruzual & Charlot 2003), which computes the spectral evolution of stellar populations from 91 \AA to 160 μm at rest. The model incorporates all of the stellar evolutionary phases and faithfully reproduces the observed optical and near-infrared color-magnitude diagrams of the Galactic star clusters with various ages and metallicities, and typical galaxy spectra from the Sloan Digital Sky Survey (SDSS) (Bruzual & Charlot 2003). It was also used to fit high-redshift galaxies with results comparable to those of other stellar population synthesis models (López-Corredoira et al. 2017; Gao et al. 2024). We adopt the 30 templates (ten ages: 0.005, 0.025, 0.10, 0.29, 0.64, 0.90, 1.4, 2.5, 5.0, 11 Gyr; three metallicities: $[M/H]=0, \pm 0.4$) of instantaneous-burst models used to fit the continua in the SDSS galaxy spectra (Tremonti 2003). The normalization of the spectra is chosen so that $L_{\text{SSP}}(\lambda=5500 \text{\AA})=1$. This means that A_2 represents the ratio of young/old rest luminosity at 5,500 \AA .

We note that the stellar population synthesis model of Bruzual & Charlot (2003) contains emission lines in the calculation of the average fluxes of each SSP, in cases where we found a very young galaxy with significant star formation. In principle, we do not expect young galaxies because the criterion we use to select our galaxies, following Labbé et al. (2023), chooses old and massive galaxies (though with a residual component of a young population). Other authors, e.g., Endsley et al. (2023), used a very different selection of galaxies, with faint UV (no Lyman- α break) and lacking a strong Balmer break, and found a significant representation in their samples of very young galaxies with star formation, but this is not our case here, as we shall see.

For the extinction law, we use an attenuation curve often utilized in high-redshift studies: Calzetti's law (Calzetti et al. 2000), derived empirically for a sample of nearby starburst (SB) galaxies containing small magellanic cloud-like dust grains. The application of this law is suggested for the central star-forming regions of galaxies, and is therefore appropriate for high- z galaxies, though some authors allow for the possibility that the JWST high- z galaxies may have different dust properties (Markov et al. 2023). For this reason, Calzetti's law is frequently used to correct the inferred SFR at high-redshift, and we use this extinction law here with the parameter $R_V = 4.05$. This law is valid for $\lambda > 1200 \text{\AA}$ at rest; for lower wavelengths, we use the theoretical model with $R_V = 4.0$ by Weingartner & Draine (2001) normalized at $\lambda = 1200 \text{\AA}$ from Calzetti's law.

The models EAZY used by Labbé et al. (2023) that provide the best fits (according to their Fig. 3) have been produced using a template set by removing the oldest stars, which is similar to other models that use universe priors. We should not use any priors. We want to test

whether the ages are compatible with standard cosmology, so we cannot assume a priori that they are younger than the Universe. And using only one single stellar population cannot simultaneously explain both the Lyman- α and Balmer breaks. Moreover, in order to produce their fits within a limited maximum age, Labbé et al. (2023) combined a dusty stellar population (producing the reddening around the Balmer break) with a young stellar population (producing the Far-UV Lyman break) without, or very little, dust.⁸ This practice of fitting V-shaped SEDs at high- z as a combination of a young, low-mass, low-attenuation galaxy (i.e., a typical Lyman-break galaxy) and, on the other, a more massive and dusty galaxy, is quite common (e.g., Barro et al. 2024). But this is not physical, because the extinction of dust (if any) should be applied to the whole stellar population, especially the youngest component that produces the Far-UV break, given that the dust is more abundant in young populations (Mallery et al. 2022). At a minimum, extinction in the young population cannot be lower than the extinction in the old population. Here we apply the same extinction to both the old and young populations.

Once we identify the free parameters that minimize the previous expression, their corresponding error bars are derived by constraining the models that follow (Avni 1976)

$$\chi_{\text{red}}^2 < \chi_{\text{red, minimum}}^2 \left[1 + \frac{f(CL, N_{\text{dof}})}{N_{\text{dof}}} \right]. \quad (2)$$

For seven free parameters and $N = 10$ ($N_{\text{dof}} = 3$ degrees of freedom), $f(CL) = 7.81$ at 2σ ; for the case of six free parameters and $N = 10$ (when the redshift is fixed; 4 degrees of freedom), $f(CL) = 9.49$ at 2σ ; for 6 free parameters and $N = 13$ (in the stacked SED; 7 degrees of freedom), $f(CL) = 8.18$ at 1σ , $f(CL) = 14.1$ at 2σ . The inclusion of the factor $\chi_{\text{red, minimum}}^2$ on the right-hand side of the inequality takes into account the fact that the errors were underestimated or overestimated when $\chi_{\text{red, minimum}}^2 \neq 1$; that is, this is equivalent to assuming that our fit is a “good fit” (with $\chi_{\text{red, minimum}}^2 \approx 1$) and multiplying the error bars by some factor to get it. For the average stacked SED, we also calculate confidence levels through a maximum likelihood algorithm or direct probability of χ^2 (see Appendix A).

There are many publicly available algorithms of SED fitting (Pacifi et al. 2023). Here we use our own algorithm instead of one of these in order to maintain better control over the different parameters being fitted: using two SSPs, using the whole range of ages instead of limiting them to be younger than the Universe, establishing global extinction rather than adding combinations of extinctions and ages that are unphysical, and deriving the error bars for the fitted parameters. In Appendix C, we carry out some calculations using one of the publicly available algorithms—the *PHARE* package—to show con-

sistency between our results and those based on other independent calculations.

3.2. Results

The best fit results for the 13 galaxies in our sample are shown in Fig. 1 and Table 1. All cases are compatible (within 95% CL) with zero extinction. The average redshift of these 13 galaxies is $\langle z \rangle = 8.2 \pm 0.4$ (1σ), at which the Λ CDM universe had an age $t_{\text{Univ}}(\langle z \rangle) = 0.61 \pm 0.04$ (1σ) Gyr. We emphasize that the age of the Universe at any given redshift depends on the cosmological model, but the age of the galaxy derived via SED fitting is totally independent of the cosmology.

We emphasize that, for the fits shown in Fig. 1 and summarized in Table 1, we have not introduced any constraint on the age of the galaxies, allowing them to be larger than the age of the Universe. Were we to limit the age of the galaxies to be younger than that of the Universe, the fits would be much worse, as we shall illustrate in appendix D.

We estimate the intrinsic (extinction-corrected) luminosity at rest in the V-filter, $L_{V,0}$, and the stellar masses of the galaxies corresponding to the SED fitting assuming for each component (old or young; the young component gives a negligible contribution to the mass) a mass-to-light ratio $M/L_{V,\text{rest}} \approx 0.6 \times \text{age}(\text{Gyr})^{0.7}$ (derived from Fig. 4 of McLaughlin & van der Marel (2005) for solar metallicity, neglecting the metallicity dependence). These numbers are given in Table 2. The order of magnitude of the stellar masses are similar to those obtained by Labbé et al. (2023). For the best fit values, we have lower extinction but larger ages than the Labbé et al. (2023) analyses, so these factors largely annul each other, give even larger masses, though we have very large error bars in the mass due to the large error bars in the ages. The ratio of young/total mass is very low, $\leq 1\%$ for the best fits, except for the galaxy ID #11184.

The weighted average (see appendix B) of $\log_{10}(\text{age}_{\text{old}})$ of these galaxies, converted to linear scale, gives

$$\langle \text{age}_{\text{old}} \rangle = 1.02_{-0.37}^{+0.53} (68.2\%CL) \quad +1.43_{-0.59} (95.4\%CL) \text{ Gyr}. \quad (3)$$

If we sum the 13 SEDs at rest (assuming the redshift inferred from their best fits) weighted in proportion to their luminosity at 4000 Å, we obtain the stacked SED plotted in Fig. 2 and summarized in Table 3, whose optimized parameters (excluding the redshift, which is fixed at zero in the rest SED) are given in Table 1 (note that the errors in this table are quoted as 95% CL, equivalent to 2σ). This stacked SED is obtained as a weighted (in proportion to the luminosity at 4000 Å) sum of SEDs at rest, $L(\lambda) = \sum_i L_i(\lambda)$. We include in the calculation of the errors the uncertainty in both the flux and the redshift:

$$(\Delta L)(\lambda) = \quad (4)$$

$$= \sqrt{\left(\sum_i \Delta L_i(\lambda) \right)^2 + \left[\frac{dL(\lambda)}{d\lambda} \left(\sum_i \frac{L_i(\lambda)}{L(\lambda)} \frac{\lambda \Delta z_i}{1 + z_i} \right) \right]^2};$$

$L_i(\lambda)$ and $\Delta L_i(\lambda)$ are derived from the linear interpolation of the available values of $L_i(\lambda_j)$ and $\Delta L_i(\lambda_j)$, with λ_j the wavelengths of the filters at rest. The stacked SED

⁸ This is shown explicitly in the first version of the arXiv preprint (<https://arxiv.org/abs/2207.12446v1>), where F_λ is plotted instead of F_ν (and the V-shape is more evident with F_λ), and the top-right panel of Fig. 3 clearly shows how they use a dusty stellar population to explain the Balmer break, and this dust does not take part in the far-UV range.

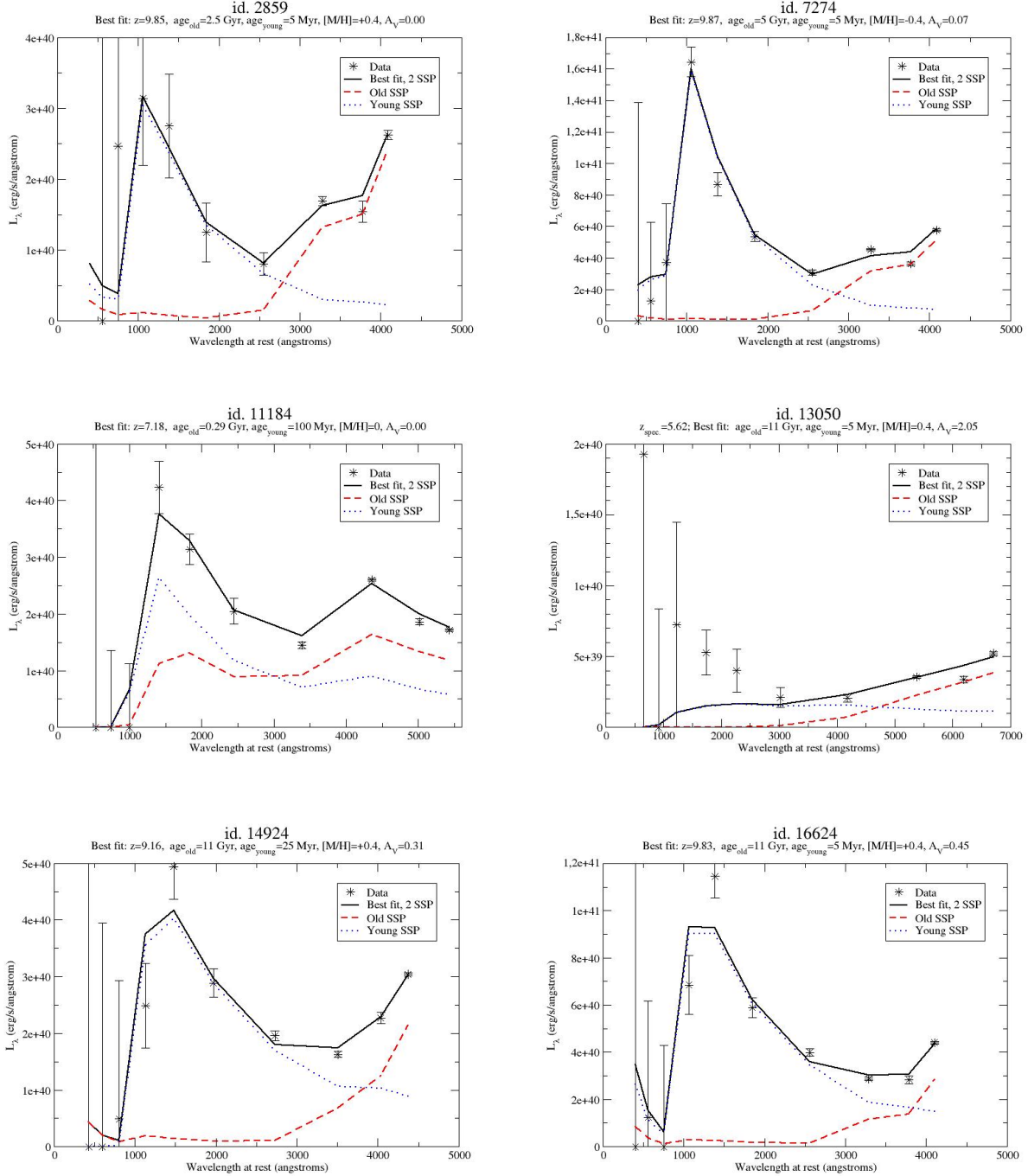


Figure 1. The best fit SEDs of the 13 galaxies in our sample, shown here at rest assuming the redshift inferred from the fitting. Negative luminosities are represented with a value of zero and its corresponding error bar.

is obtained in bins of 500 \AA , approximately the same as the average resolution of each SED at rest.

If we sum the 4 SEDs at rest of only the galaxies with available spectroscopic redshift weighted in proportion to their luminosity at 4000 \AA we obtain the stacked SED plotted in Fig. 3 and summarized in Table 3, whose optimized parameters (excluding the redshift, which is fixed at zero in the rest SED) are given in Table 1.

The most interesting parameter of this fit of stacked

SED with 13 galaxies is the age of the oldest population, which is constrained by Eq. (2) to be:

$$\text{age}_{\text{old, stacked}} \geq 1.6 \text{ Gyr (68\%CL)}, \geq 0.9 \text{ Gyr (95\%CL)}, \quad (5)$$

in agreement with the previous estimate of the weighted average for the minimum age. Using other likelihood estimators (see Table 4), the probabilities of the young population are even lower. For instance, using a maxi-

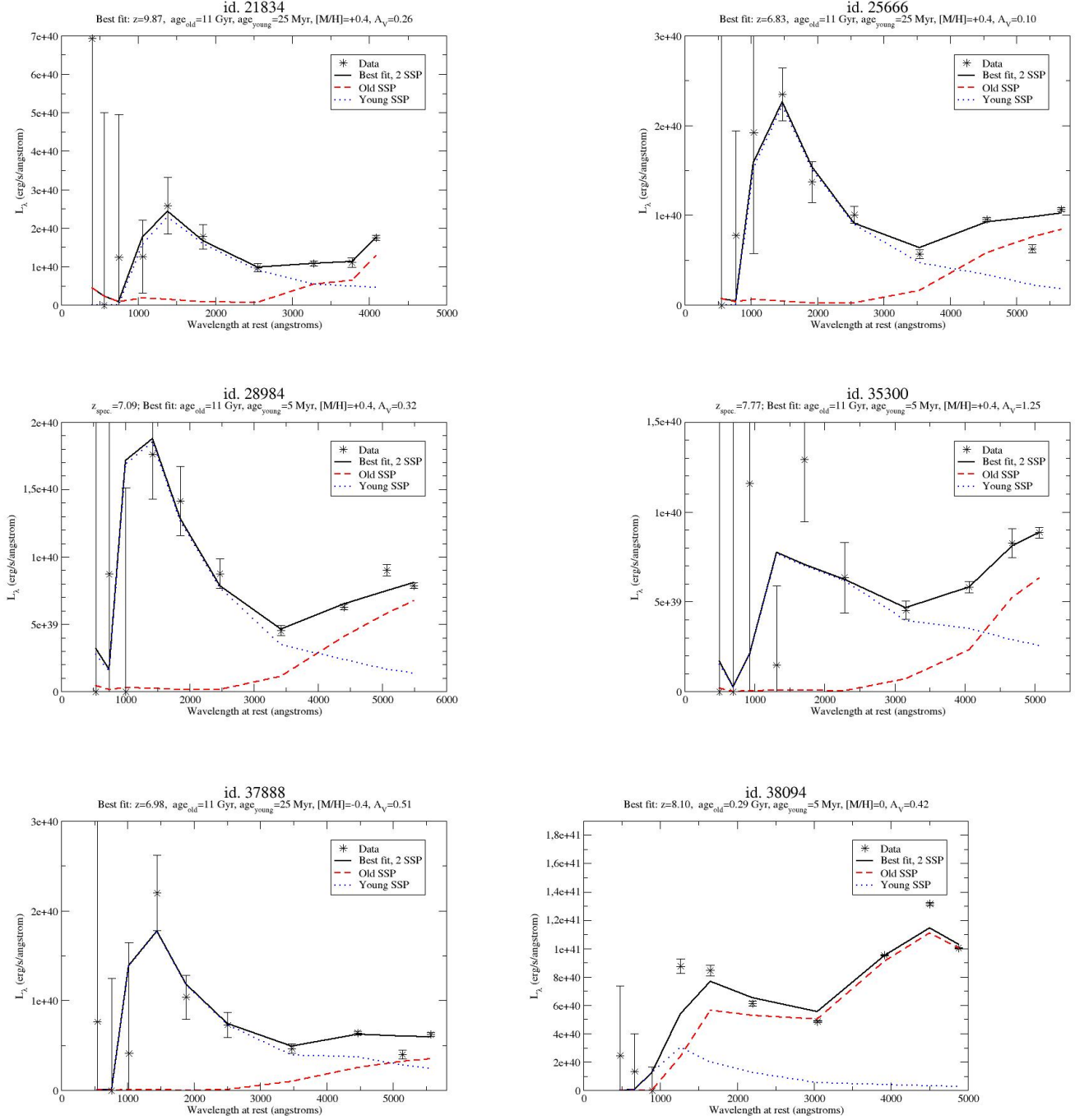


(Fig. 1 cont.)

imum likelihood approach (see Appendix A) gives tighter constraints: $\text{age}_{\text{old,stacked}} \geq 3.9$ Gyr (68%CL), ≥ 2.1 Gyr (95%CL). We keep the result based on Equation (2) since it is more conservative (for it allows a wider range of ages). The same exercise stacking only the four galaxies with spectroscopic redshifts gives almost the same results: $\text{age}_{\text{old,stacked spec.}} \geq 1.9$ Gyr (68% CL), $\text{age}_{\text{old,stacked spec.}} \geq 0.9$ Gyr (95% CL).

For $\lambda_{\text{rest}} \geq 5500$ Å, only 1-3 galaxies contributed to the stacked SED (only 1 in the case of the stacking with spectroscopic redshift). We may think that the galaxy or galaxies contributing to $\lambda_{\text{rest}} \geq 5500$ Å (with the lowest redshifts) are special cases different from the rest of the sample. However, if we restrict our fits of the SED fitting to $\lambda_{\text{rest}} \leq 5000$ Å or $\lambda_{\text{rest}} \leq 4000$ Å, we get very similar results of the fit (see last rows of Table 1).

Note that the errors may be approximately Gaussian

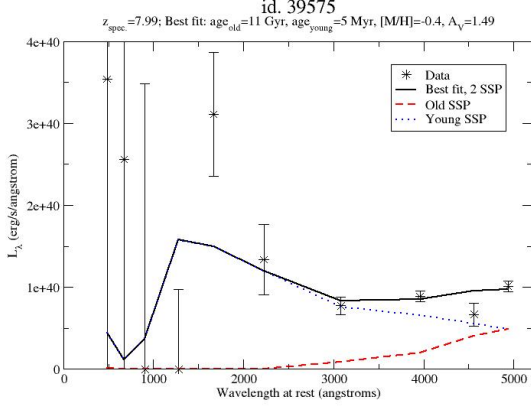


(Fig. 1 cont.)

Table 2

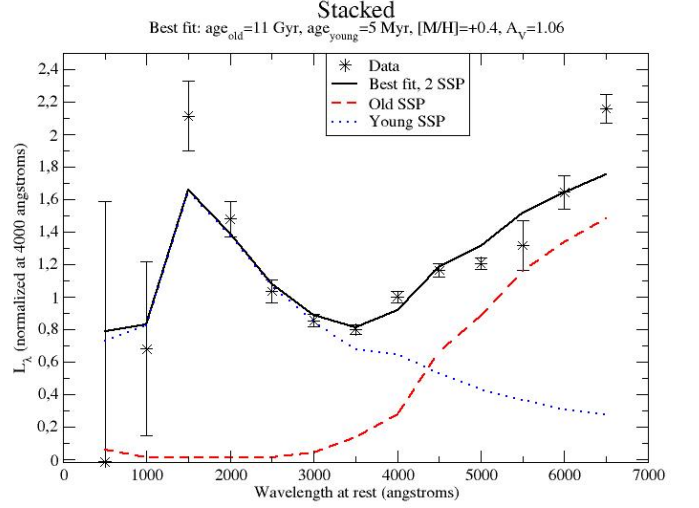
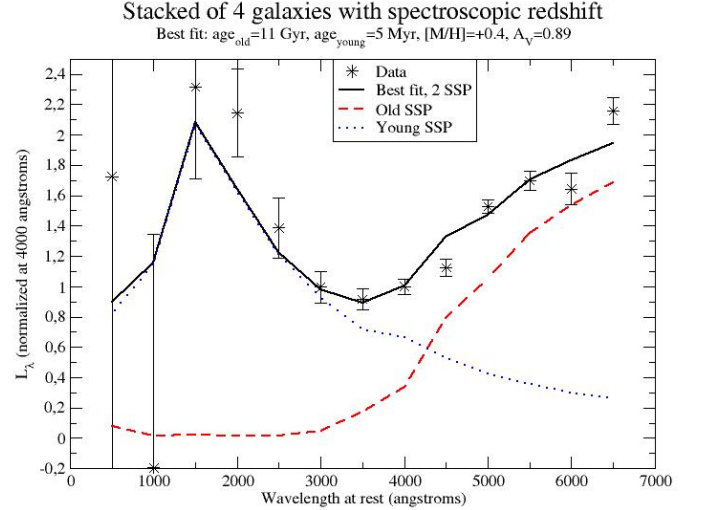
$L_{V,0}$ is the intrinsic (extinction-corrected) luminosity in filter V-rest. M is the total (young+old) stellar mass. The last column indicates the ratio of young/total mass. Error bars correspond to 95% CL.

Galaxy ID	$L_{V,0}(L_{\odot})$	$M(M_{\odot})$	M_{young}/M
2859	1.1E10	$1.2^{+2.1}_{-0.7}$ E10	$0.03^{+0.20}_{-0.03}\%$
7274	2.2E10	$3.9^{+2.9}_{-3.8}$ E10	$0.03^{+0.44}_{-0.03}\%$
11184	3.8E9	$8.0^{+5.4}_{-4.2}$ E8	$19^{+17}_{-19}\%$
13050	3.6E10	$7.7^{+3.5}_{-7.2}$ E10	$0.2^{+30}_{-0.2}\%$
14924	1.8E10	$5.2^{+0.3}_{-4.9}$ E10	$0.16^{+0.49}_{-0.14}\%$
16624	4.5E10	$1.3^{+0.1}_{-1.3}$ E11	$0.04^{+0.33}_{-0.04}\%$
21834	3.5E10	$4.1^{+0.1}_{-3.5}$ E10	$0.09^{+0.21}_{-0.08}\%$
25666	2.8E9	$7.5^{+1.6}_{-7.2}$ E9	$0.3^{+12}_{-0.2}\%$
28984	3.5E9	$9.4^{+1.2}_{-8.4}$ E9	$0.08^{+0.84}_{-0.08}\%$
35300	2.3E10	$5.9^{+1.1}_{-5.3}$ E10	$0.12^{+2}_{-0.12}\%$
37888	3.5E9	$6.7^{+3.7}_{-6.7}$ E9	$1.0^{+4}_{-1.0}\%$
38094	4.3E10	$1.1^{+12}_{-0.8}$ E10	$0.13^{+5}_{-0.13}\%$
39575	3.6E10	$7.1^{+2.7}_{-7.1}$ E10	$0.3^{+11}_{-0.3}\%$

Table 3

Stacked SED at rest for the 13 galaxies, and for the 4 galaxies with spectroscopic redshift. Fluxes are normalized to unity at 4000 Å. N is the number of galaxies that have some contribution in the bin; N_{sp} is the number of galaxies with spectroscopic redshift that have some contribution in the bin.

$\lambda_{\text{rest}}(\text{Å})$	N	N_{sp}	$\langle F_{\lambda} \rangle$ (all)	$\langle F_{\lambda} \rangle$ (spec. gal.)
500	13	4	-0.014 ± 1.599	1.726 ± 4.487
1000	13	4	0.679 ± 0.535	-0.194 ± 1.541
1500	13	4	2.112 ± 0.214	2.316 ± 0.606
2000	13	4	1.479 ± 0.110	2.144 ± 0.291
2500	13	4	1.034 ± 0.072	1.387 ± 0.199
3000	13	4	0.853 ± 0.039	0.996 ± 0.106
3500	13	4	0.800 ± 0.030	0.917 ± 0.072
4000	13	4	1.000 ± 0.035	1.000 ± 0.049
4500	8	4	1.163 ± 0.040	1.125 ± 0.056
5000	6	3	1.207 ± 0.035	1.529 ± 0.042
5500	3	1	1.316 ± 0.151	1.698 ± 0.063
6000	1	1	1.643 ± 0.103	1.643 ± 0.103
6500	1	1	2.158 ± 0.088	2.158 ± 0.088

**Figure 2.** Best fit using two SSPs of the stacked SED at rest ($\chi_{\text{red}}^2 = 6.34$). Data in Table 3.**Figure 3.** Best fit using two SSPs of the stacked SED at rest of only the four galaxies with spectroscopic redshift ($\chi_{\text{red}}^2 = 4.08$). Data in Table 3.

for $\log_{10}(\text{age}_{\text{old}})$, but not for age_{old} . We estimate the probability of fitting the stacked SED of all the galaxies with an $\text{age}_{\text{old}} \leq 290$ Myr to be 3×10^{-4} , (derived from the $\chi_{\text{red}}^2 = 31.25$ of the best fit using $\text{age}_{\text{old}} \leq 290$ Myr; much larger than the corresponding $\chi_{\text{red}}^2 = 6.34$ for the best fit using $\text{age}_{\text{old}} \leq 11$ Gyr). This would be equivalent to a 3.6σ event. Based on a maximum likelihood approach (Appendix A), it would reach 4.9σ . The probability of fitting the stacked SED with an $\text{age}_{\text{old}} \leq 640$ Myr is 1.8×10^{-3} , derived from the $\chi_{\text{red}}^2 = 27.19$ of the corresponding best fit (see the left panel of Fig. 4), which would be equivalent to a 3.1σ event in the most conservative calculation. It is 2.4σ for the stacked SED with

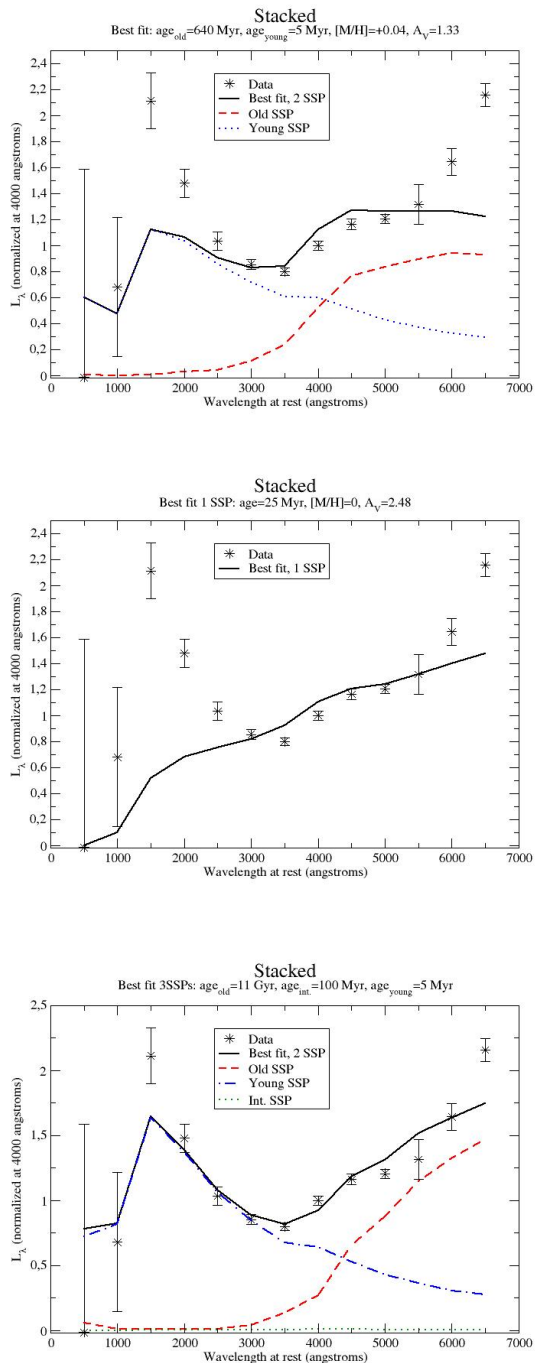


Figure 4. Best fit of the stacked SED at rest: Left panel: two SSPs with $\text{age}_{\text{old}} \leq 640$ Myr ($\chi^2_{\text{red}} = 27.19$); Middle panel: one SSP ($\chi^2_{\text{red}} = 24.30$); Right panel: three SSPs assuming $[M/H] = +0.4$, $A_V = 1.06$ ($\chi^2_{\text{red}} = 6.36$).

four spectroscopic galaxies.

A fit of this stacked SED with one SSP would yield much worse results in comparison with two SSPs, as may be seen in the middle panel of Fig. 4. One cannot fit both breaks at the same time with only one population. Increasing the number of SSPs beyond two does not improve the fit significantly. For instance, an optimized SED with three SSPs (while keeping the extinction and

metallicity at their best fit values for two SSPs, in order to keep the same number of free parameters) produces almost the same best-fit value of the oldest population and its lower age limit, shown in the right panel of Fig. 4. Evidently, the third age produces only a very small additional contribution to the young population. This reinforces our previous claim that exponentially decaying, extended star formation models do not fit these V-shaped SEDs. Nonetheless, a more accurate determination of extinction models and templates of SSPs, and with more precise values of ages and metallicities instead of the discrete values we have used, might improve the fits.

To check the consistency of our calculations with those based on publicly-available SED fitting packages, we compare in Appendix C our results with those produced by *le PHARE*. These yield similar conclusions regarding the necessity of including an old population to fit the data.

Our assumptions may harbor other systematic errors: neglecting the light contamination from other galaxies or the assumption of a standard IMF, and the presumed extinction law. The super-solar metallicities in the GALAXEV model are produced by interpolating the grids, which might yield some systematic error in the star-formation histories and hence the ages. From our analysis, however, we can see that the metallicity is not a significant factor in the SED fitting. But these possible uncertainties should not prevent us from seeing the fundamental outcome: it is not possible to fit the observed SED with a pure young population because of the clear existence of the V-shape (with pronounced wings) and a Balmer break (López-Corredoira et al. 2017) and red color at longer wavelengths (López-Corredoira 2010).

In addition, the amplitude of the Balmer break, which is strongly dependent on age (Steinhardt et al. 2023), necessarily should have ~ 1 Gyr-old populations, though some authors believe that the JWST high- z galaxies are compatible with the prediction of simulations using the standard cosmological model (Vikaeus et al. 2024). The possibility of explaining the Balmer break in double-break galaxies with emission lines (Desprez et al. 2024) is already contained in our fits because the Bruzual & Charlot (2003) stellar population models contain the possibility of including any fraction of a young population, which includes emission lines.

Other results obtained with similar methods of SED fitting by Rocca-Volmerange et al. (2018) also yield quite high ages at very high redshifts: a 450-500 Myr-old galaxy at $z = 8.6$ and a ~ 160 Myr-old galaxy at $z = 11.1$.

3.3. Understanding the results

One may suspect that the numerical SED fitting may have errors that produce the result that the galaxy must be old, even if our analysis includes an independent check using different software (Appendix C). When using a code as a black box that receives some input and delivers some output, strange results can arise if the algorithm has errors. It is therefore useful to understand and interpret the physical meaning of any numerical result and the reason it is derived. As we have already noted on several occasions, the key issue to understand with our analysis is that the large ages we infer for the old stellar popula-

tion are constrained by the Lyman break to have small extinction, so reddening can affect the Balmer break only by a small amount as well. But we have red color around the Balmer break which, in the absence of large extinction, can thus be due solely to an old population. Let us confirm this with a rough calculation of the V-shaped SED.

The first element is that the far-UV can only be explained with a very young population; an old population makes only a negligible contribution there. If we take our stacked spectrum of 13 galaxies in Fig. 2 (as we have seen previously, there is no reason to suspect that errors in the photometric redshift produce important artefacts in the stacked SED at rest, because we get the same SED using only the 4 galaxies with spectroscopic redshift), we measure $\frac{F_\lambda(1500 \text{ \AA})}{F_\lambda(3000 \text{ \AA})} = 2.48 \pm 0.23$.

Hence, $m_{\text{AB,rest:1500-3000 \AA}} = 0.52 \pm 0.10$. This is a relatively blue color in the far-UV and is expected because the selection criteria used to choose these 13 galaxies include the constraint $F150W-F277W < 0.7$ which, at an average redshift of $z = 8.2$, is equivalent to setting $m_{\text{AB,rest:1630-2980 \AA}} < 0.7$.

Let us ignore the dependence on metallicity, which is low as we have seen, and also neglect any possible AGN contamination which, as we shall confirm in the next subsection, is also low. We consider only solar metallicity here. Then, assuming an age of 5 Myr for the young population to fit the far-UV signal, for which $m_{\text{AB,rest:1500-3000 \AA}}[\text{SSP:5 Myr}] = -0.34$ and given the reddening implicit in Calzetti's law, $E(\text{rest} : 1500 - 3000 \text{ \AA}) = 0.72A_V$, we get $A_V = \frac{0.52 - (-0.34)}{0.72} = 1.19$ (quite close to the result of our SED fitting corresponding to Fig. 2). This is the maximum extinction, because for a larger age of the young population, the intrinsic color is redder, thus yielding a smaller A_V . Therefore, it makes sense to claim that our average A_V is, at most, one magnitude, for otherwise the far-UV region would be redder and the Lyman-break might even vanish.

How big should our young population be to fit this Lyman break? We know that at 1500 \AA at rest the contribution from the old population is negligible and, comparing it with the relative flux at the V-rest filter, we derive (using Eq. 1, bearing in mind the normalization $L_{\text{SSP}}[\lambda = 5500 \text{ \AA} \equiv V] = 1$, and adding Calzetti's law extinction),

$$\frac{L_\lambda(1500 \text{ \AA})}{L_{\lambda,V}} = \frac{A_2 L_{\lambda,\text{young}}(1500 \text{ \AA})}{1 + A_2} 10^{-1.55A_V/2.5}, \quad (6)$$

so that

$$A_2 = \left[\frac{L_{\lambda,\text{young}}(1500 \text{ \AA}) \times 10^{-1.55A_V/2.5}}{\frac{L_\lambda(1500 \text{ \AA})}{L_{\lambda,V}}} - 1 \right]^{-1}. \quad (7)$$

In our stacked SED, we measure $\frac{L_\lambda(1500 \text{ \AA})}{L_{\lambda,V}} = 1.60 \pm 0.25$.

Next, we analyze the redder wavelengths and consider the color $(B - V)_{\text{AB}}$. For the combination of two SSPs we have adopted, we get

$$(B - V)_{\text{AB}} = (B - V)_{\text{AB,old}} + E(B - V) \quad (8)$$

$$-2.5 \log_{10} \left(\frac{1 + A_2 \frac{L_{\lambda,B,\text{young}}}{L_{\lambda,B,\text{old}}}}{1 + A_2} \right).$$

The reddening with Calzetti's law is $E(B - V) = 0.247A_V$. The third term on the righthand side gives the blueing due to the young population's contribution, and depends on the calculated fractions of young and old components. The young population is always bluer than the old population, so this term is always negative. The value of this third term falls within the limits $(-0.54, -0.18)$, consistent with range of ages compatible with the global color, as we shall see in the next paragraph.

In the stacked SED, we measure $\frac{F_\lambda(4400 \text{ \AA})}{F_\lambda(5500 \text{ \AA})} = 0.78 \pm 0.04$, for which $(B - V)_{\text{AB}} = 0.74 \pm 0.06$. Again, this is expected because we have preselected red galaxies through the condition $F277W-F444W > 1.0$, equivalent (at average redshift $z = 8.2$) to $m_{\text{AB,rest:2980-4830 \AA}} > 1.0$. If one were to include only extinction-correction and ignore the blueing of the young population, the result would be $(B - V)_{\text{AB,old}} > 0.45 \pm 0.06$, equivalent in Vega calibration to $(B - V)_{\text{Vega,old}} > 0.57 \pm 0.06$. The blueing of the young stellar population would make the old population even redder, with a larger $(B - V)_{\text{Vega,old}}$ and never smaller. This color is associated with a stellar population older than 1 Gyr (López-Corroira 2010, Fig. 2). A population younger than 0.5 Gyr would require $(B - V)_{\text{Vega,old}} < 0.35$, which cannot be obtained with these data. The fact that our preferred solution (though with a very generous error bar) includes the oldest population is due to the fact that the data favor the value $(B - V)_{\text{Vega,old}} \approx 1.1$, for which the third term in Eq. (8) contributes with a value of -0.5, though a broad range, $(B - V)_{\text{Vega,old}} > 0.57$, is possible.

In other words, in order to make the observed red color after the Balmer break compatible with an age of the oldest population lower than 0.5 Gyr, we would need to make $(B - V)_{\text{Vega,old}} < 0.35$ and an extinction $A_V \gtrsim 2.1$, which would make $E(\text{rest} : 1500 - 3000 \text{ \AA}) \gtrsim 1.5$, $m_{\text{AB,rest:1500-3000 \AA}} \gtrsim 1.2$, so we would not see the Lyman break. Of course, this is forbidden by our data that a priori have a selection with $m_{\text{AB,rest:1630-2980 \AA}} < 0.7$.

3.4. AGN contamination

There are several color criteria for selecting AGNs in high redshift samples: some of them use infrared mid-infrared colors (Assef et al. 2010), or are also especially designed for JWST near-infrared filters (Goulding & Greene 2022). These criteria are not applicable to our particular selection of galaxies, however, because: (i) we do not have photometry beyond $5 \mu\text{m}$; (ii) our galaxies were selected to be very red and provide an important Balmer break, so we cannot use the filters F356W, F444W; and (iii) though the filters F150W, F200W, F277W might be used as criteria for the JWST filters (Goulding & Greene 2022), this is only practical when the signal/noise is relatively high, which is not our case here.

An important AGN component could modify the fitted parameters and also the mass of the galaxy, but it is

not expected in our sample. AGNs are extremely blue in the range below $\sim 1000 \text{ \AA}$ at rest, unless there is a huge extinction, which is not expected because otherwise we could not see the Lyman break. Strong emission lines, a dusty continuum and AGN contributions together could explain this Lyman break (Windhorst et al. 2023), but our model contains all of these elements and does not favor this solution, as we shall see below. We again note that emission lines are already included in the young population templates in the GALAXEV model, and lines are also included in the AGN template we shall use.

The sample of 13 galaxies selected by Labbé et al. (2023) already removed most of the strongly dominant AGNs by requiring that they were not detected in the HST filters [SNR(F435W, F606W, F814N) < 2] (equivalent to $\lambda \lesssim 1000 \text{ \AA}$ at rest for an average redshift of $z = 8$). There may be still be some possible small component of AGN or active galaxy with small black hole mass, however. As a matter of fact, one of those galaxies (id. 13050) has already been identified as an AGN with a low-mass ($\sim 10^7 M_\odot$) black hole at $z = 5.62$ via a follow-up spectroscopic observation (Kocevski et al. 2023). The noise in HST filters is even higher than in JWST filters, so some emission at $\lambda \lesssim 1000 \text{ \AA}$ at rest may be hidden. An AGN component would make a blue contribution around the Balmer break, so it cannot explain the large Balmer break we observe here, and the higher the AGN component, the larger the age of the oldest population necessary to redden the Balmer break (apart from extinction), so it will not affect our calculations of the minimum age of the oldest population. Nevertheless, we shall carry out a fit of the stacked SED including an AGN component to check that it does not affect our results.

In this additional fit, we assume the usual two SSPs of stellar population plus an extra AGN component with fixed characteristics (so there are no extra free parameters):

$$F_{\text{theor.}}(\lambda_i) = \frac{L_0}{4\pi d_L(z)^2(1+z)} \quad (9)$$

$$\times [\langle L_{\text{SSP}}(\text{age}_{\text{old}}, [\text{M}/\text{H}], A_V; \lambda/(1+z)) \rangle_T$$

$$+ A_2 \langle L_{\text{SSP}}(\text{age}_{\text{young}}, [\text{M}/\text{H}], A_V; \lambda/(1+z)) \rangle_T$$

$$+ A_3 \langle L_{\text{AGN}}(A_{V,\text{AGN}}; \lambda/(1+z)) \rangle_T],$$

where L_{AGN} is obtained from Assef et al. (2010), normalized such that $L_{\text{AGN}}(A_V; 5500 \text{ \AA}) = 1$, and A_3 represents the ratio of AGN/old rest luminosity at 5500 \AA when the extinction for AGN and stars is the same. Fig. 5 shows the best fit of the stacked SED at rest for $A_3 = 0.0045, 0.023, 0.090$ including the same extinction that affects the stellar populations ($A_{V,\text{AGN}} = A_V$), characterized by $\chi_{\text{red}}^2 = 6.41, 7.01, 10.98$ respectively, and with an age of the oldest population equal to 11 Gyr in all cases. Fig. 6 shows the best fit of the stacked SED at rest for $A_3 = 0.0045, 0.023, 0.090$ without any extinction for the AGN component, characterized by $\chi_{\text{red}}^2 = 7.87, 21.04, 52.86$ respectively, and with an age of the oldest population equal to 5 – 11 Gyr. Fig. 7 shows the best fit of the stacked SED at rest for $A_3 = 0.127, 0.575, 5.81$ with a heavy extinction for the AGN component, $A_{V,\text{AGN}} = 3$, representing a red QSO (Calistro Rivera et al. 2021),

characterized by $\chi_{\text{red}}^2 = 6.65, 11.28, 26.25$ respectively, and with an age of the oldest population equal to 11 Gyr.

A usual blue AGN with small extinction component makes the flux bluer around the Balmer break, which requires an even greater age for the galaxy, or increasing the reddening of the stellar population through extinction, but this is limited due to the presence of the Far-UV features, especially the bin of 500 \AA at rest (equivalent to the observed flux in the filter HST/F435W).

A red/heavily-extincted AGN may help to explain the red color near the Balmer break, but its amplitude would also be limited by the flux at 500 \AA at rest, which not even heavy extinction can remove. This is due to the strong decrease in extinction below 800 \AA and a heavy increase in the intrinsic luminosity at these wavelengths: $L_{\text{AGN}}(A_V = 0; 500 \text{ \AA}) = 260 L_{\text{AGN}}(A_V = 0; 5500 \text{ \AA})$, $A_{500\text{\AA}} = 2.5 A_V$, whereas $L_{\text{AGN}}(A_V = 0; 800 \text{ \AA}) = 95 L_{\text{AGN}}(A_V = 0; 5500 \text{ \AA})$, $A_{800\text{\AA}} = 5.1 A_V$. Thus, even with a heavy extinction of $A_V = 3$, we get $L_{\text{AGN}}(A_V = 0; 500 \text{ \AA}) \sim 4 L_{\text{AGN}}(A_V = 0; 5500 \text{ \AA})$, even higher when we take an average over the wavelengths within the wide filter. Moreover, a heavily extincted QSO dominating the flux contribution would need a very large intrinsic luminosity of the QSO (to compensate for the extinction). In our example with the largest QSO contribution and largest extinction (Fig. 7 with $A_3 = 5.82$), we would need an intrinsic QSO luminosity $L_{0.300-6500 \text{ \AA}} \sim 10^{47}$ erg/s, which requires a massive black hole whose formation would conflict with the short timeline available at $z \approx 8$ within standard cosmology. This is not necessarily impossible, since something similar has already been observed (Wang et al. 2021), but not with such an exotic combination of extinction plus an extinction-free galaxy.

Summing up, an AGN component does not help to solve the tension, but actually makes it even worse.

Other analyses (Kocevski et al. 2023; Barro et al. 2024) seem to suggest solutions involving AGN components with no extinction near the Lyman-break and heavy extinction near the Balmer break. This hybrid incorporates a young galaxy free of extinction and a heavily obscured and red QSO, or a blue QSO plus a dusty galaxy and a pure QSO plus a torus or similar exotic multicomponent galaxies that have never been observed in a single object at low z .

Certainly, if we have more free parameters in a model than the number of data, we might be able to fit anything, but it is not clear whether these solutions represent real single galaxies. In any case, even these exotic configurations are confronted with problems: a blue/unextincted QSO is excluded by the non-detection of the galaxies in the filter HST/F435W (which is not used in Kocevski et al. (2023); Barro et al. (2024)); a red QSO might be produced by heavy extinction in the nuclear volume (Calistro Rivera et al. 2021) but, as we have seen, this would also leave a very significant imprint in the filter HST/F435W. The non-detection in the filter HST/F435W is the key to excluding the strong AGN contribution hypothesis.

4. DISCUSSION

Our overall analysis, combining Equations (3) and (5), yields a galaxy age, age_{old} , between 0.9 and 2.4 Gyr

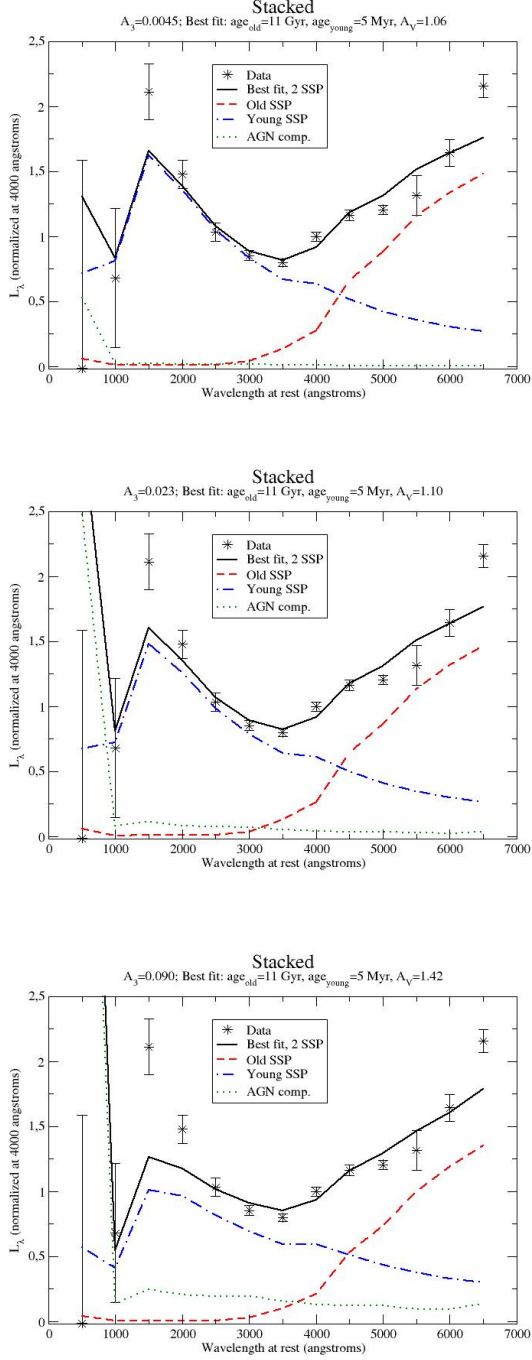


Figure 5. Best fit of the stacked SED at rest including an AGN component with $A_3 = 0.0045, 0.023, 0.090$, respectively, and the same extinction ($A_{V,AGN} = A_V$) that affects the stellar populations.

at 95.4% CL, and between 0.65 and 3.80 at 99.7% CL. Galaxies within $2 < z < 4$ with V-shaped SED and similar colors at rest have also been analyzed with the same technique, and it was concluded that for the galaxies with $z > 2.5$ there is no significant evolution of their average age, with all average ages of galaxies mostly remaining between 1 and 2 Gyr (Gao et al. 2024). Apparently, JWST has observed at $z = 8$ the same type

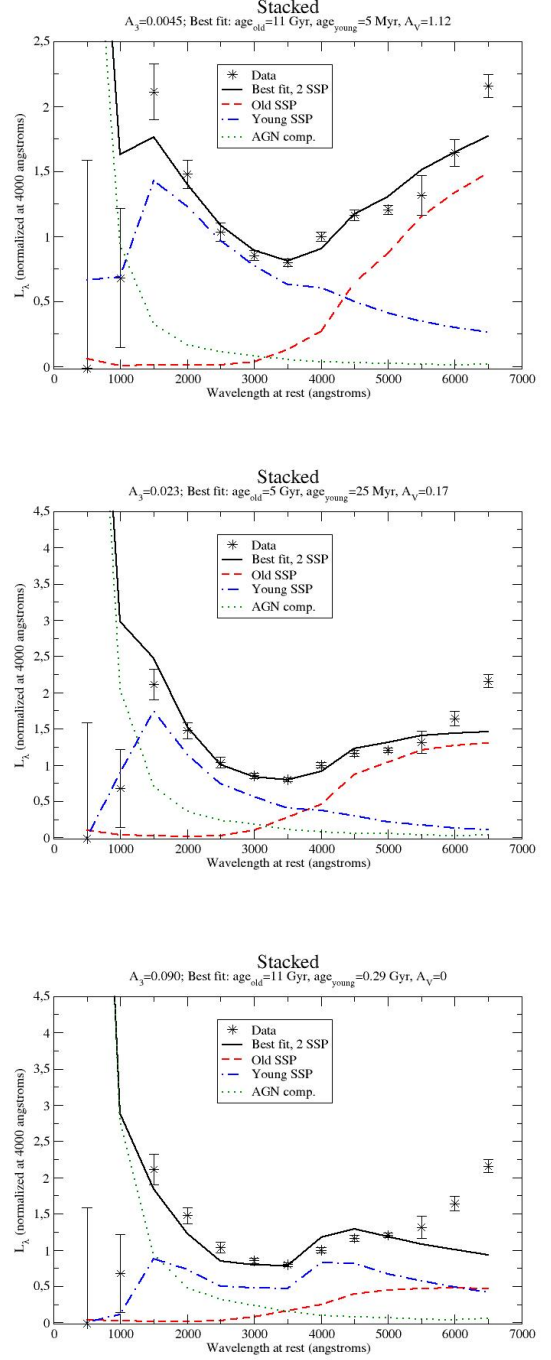


Figure 6. Best fit of the stacked SED at rest including an AGN component without extinction, $A_{V,AGN} = 0$, and with $A_3 = 0.0045, 0.023, 0.090$, respectively.

of galaxies and with the same ages than those ones analyzed with ZFOURGE data by Gao et al. (2024) within $2.5 < z < 4.0$.

The new JWST observations have thus uncovered, not only many galaxy candidates with photometric redshifts larger than 10 (e.g., Melia 2023; Franco et al. 2023; Whittler et al. 2023; Glazebrook et al. 2023; Curtis-Lake et al. 2023), but also the very massive galaxies we have analyzed in this paper that are older than the Universe in

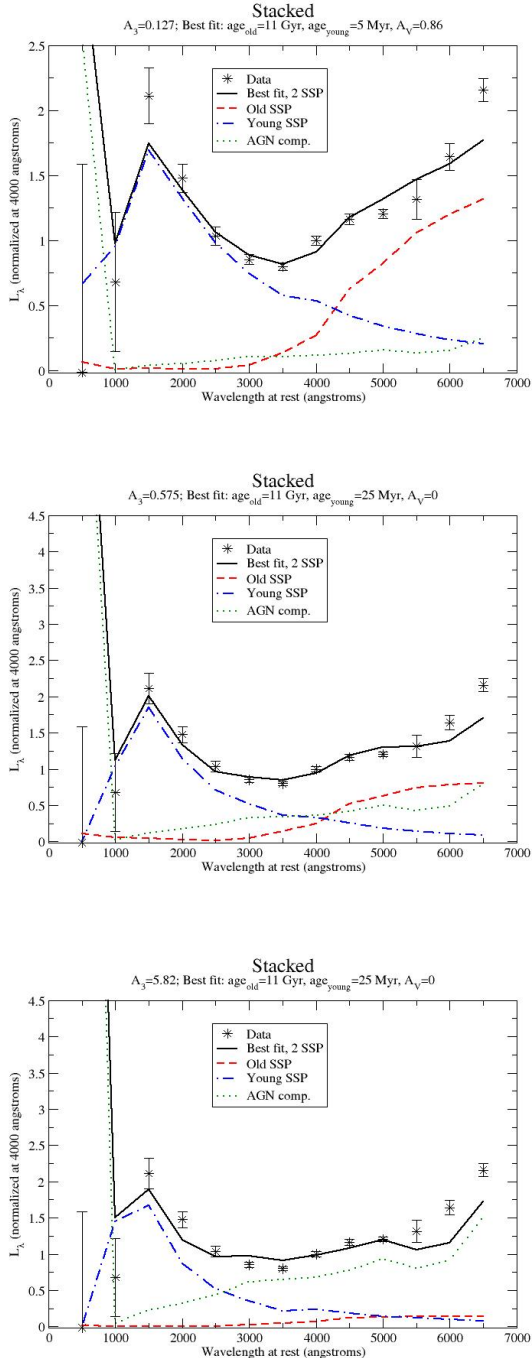


Figure 7. Best fit of the stacked SED at rest including an AGN component with extinction, $A_{V,AGN} = 3$, and $A_3 = 0.127, 0.575, 5.82$, respectively.

the context of Λ CDM within $\approx 95\%$ CL or, in any case, within $> 99.9\%$ CL, formed well beyond $z = 10$. This more robust sample of structures provides even tighter constraints on galaxy formation theory in Λ CDM, particularly from the more compelling estimate of their photometric redshifts based on the two breaks in their SED. These results conflict with semi-analytical Λ CDM models claiming that very massive galaxies formed much later (Guo et al. 2011).

The principal difficulty facing the standard model in accounting for the very early emergence of galaxies has typically been addressed by enhancing star formation, the growth of halos, stochasticity or evolving initial mass functions in the early Universe (Finkelstein et al. 2023). But the JWST observations have pushed the threshold for these processes too uncomfortably close to the big bang itself. We appear to have exhausted any flexibility left in understanding how the primordial plasma could have cooled and condensed rapidly enough to form these structures by ~ 300 Myr in the context of Λ CDM (Melia 2023). Without much doubt, some significant new physics would be required to adequately explain how such massive structures could have formed so quickly in the Λ CDM Universe.

Modelling the extinction of high- z galaxies with a dust similar to local galaxies may require a reexamination (Markov et al. 2023), though the effects are expected to be small since all our fits are compatible with no extinction; indeed the presence of Lyman- α breaks at far-UV indicates that we should have very little amount of dust, whatever their properties are. In any case, it is important to remark that using mathematical fitting models with much lower amounts of dust around young populations than is assumed for the old populations is unphysical, and here we have avoided it.

Stellar population synthesis is based on models, but we must also bear in mind that the assumed cosmology is itself only a working model, and should be viewed as being just as adjustable as stellar formation theory. Though one may question the validity of the GALAXEV templates to accurately represent the stellar populations of a given age and other assumptions, one can argue that cosmology itself is no more robust than stellar astrophysics. Assuming that our calculations are correct, we do not believe that it is far more likely for the stellar astrophysics and the other assumptions and approximations we have used throughout this paper to be flawed rather than the cosmology. In order to know whether one or the other is more likely, we would need to calibrate their probabilities based on sound statistics. For instance, what is the probability that the GALAXEV models (or any other Stellar Population Synthesis model, such as the GISELL library with a Salpeter IMF that was also used in the appendix C) are incorrect? Thus far, these stellar synthesis models have worked well in fitting observations of local galaxies and are consistent with our current knowledge of stellar astrophysics. Though these approximations may deviate significantly from reality, we cannot calculate how likely that is.

The standard model of cosmology accounts rather well for many observations, but there are also many instances that create (sometimes significant) tension with the predictions of Λ CDM (e.g., López-Corredoira 2022). The probability of Λ CDM being correct can only be determined a posteriori, once we definitively solve the puzzle of the Universe. In the end, astrophysics is a science largely based on 'orders of magnitude', not the fine precision of some theories tested in laboratories on Earth. The work we have reported here relies on several approximations that need to be tested further before we can conclude that standard cosmology is wrong.

Of course, not all alternatives to Λ CDM fare better. For example, were we to consider a cosmology with-

out dark energy, such as Einstein-de Sitter, the problem would be worse. In this cosmology, $\langle z \rangle = 8.2 \pm 0.4$ (1σ) would correspond to an age $t_{\text{Univ}}(\langle z \rangle) = 0.33 \pm 0.02$ (1σ) Gyr, which would also lead to a nonsensical time of birth for the JWST galaxies prior to the big bang within a $> 99\%$ CL.

Other cosmological scenarios might account for these observations better than Λ CDM, however. For example, the $R_h = ct$ universe (Melia & Shevchuk 2012; Melia 2020; 2023) gives an age of the Universe of 14.6 Gyr, or Covarying Coupling Constants+ Tired-light (CCC+TL) hybrid model (Gupta 2023) gives an age of the Universe of 26.7 Gyr (though difficult to reconcile with the age of the oldest known sources, in our opinion). In the most reasonable alternative, i.e., the $R_h = ct$ universe, the timeline at $z \gtrsim 6$ is approximately twice as long as that in the standard model, assuming $H_0 = 70 \text{ km s}^{-1} \text{ Mpc}^{-1}$. In this cosmology, $\langle z \rangle = 8.2 \pm 0.4$ (1σ) corresponds to an age $t_{\text{Univ}}(\langle z \rangle) = 1.51 \pm 0.07$ (1σ) Gyr, which leads to $z_{\text{form}} \gtrsim 21$ (95.4% CL) ($t_{\text{Univ}}(z_{\text{form}}) < 0.61$ Gyr). This provides a suitable scenario where these massive galaxies started forming enough time after the Pop III stars are believed to have first appeared. Together with also providing an explanation for how the earliest (though less massive) galaxies would have emerged by $z \sim 17$ ($t_{\text{Univ}} \sim 0.8$ Gyr) (Melia 2023), the longer time afforded the evolution of the most massive galaxies in this model may solve the growing puzzle of how structure formed in the early Universe.

We are grateful to the anonymous referee and the editor, Christopher Conselice, for very helpful comments that have lead to an improved presentation of the results in this paper. MLC's research is supported by the Chinese Academy of Sciences President's International Fellowship Initiative grant number 2023VMB0001 and the grant PID2021-129031NB-I00 of the Spanish Ministry of Science (MICIN). JJW is supported by the Natural Science Foundation of China (grant No. 12373053), the Key Research Program of Frontier Sciences (grant No. ZDBS-LY-7014) of Chinese Academy of Sciences, and the Natural Science Foundation of Jiangsu Province (grant No. BK20221562).

REFERENCES

- Arnouts, S., Cristiani, S., Moscardini, L., et al. 1999, *MNRAS*, 310, 540
- Arnouts, S., Moscardini, L., Vanzella, E., et al. 2002, *MNRAS*, 329, 355
- Assef, R. J., Kochanek, C. S., Brodwin, M., et al. 2010, *ApJ*, 713, 970
- Avni, Y. 1976, *ApJ*, 210, 642
- Barro, G., Pérez-González, P. G., Kocevski, D. D., et al. 2024, *ApJ*, 963, 128
- Boylan-Kolchin, M. 2023, *Nature Astron.*, 7, 731
- Bruzual, G., & Charlot, S. 2003, *MNRAS*, 344, 1000
- Calistro Rivera, G., Alexander, D. M., Rosario, D. J., et al. 2021, *A&A*, 649, A102
- Calzetti, D., Armus, L., Bohlin, R. C., et al. 2000, *ApJ*, 533, 682
- Cardiel, N., Gorgas, J., Sánchez-Blázquez, P., et al. 2003, *A&A*, 409, 511
- Conroy, C. 2013, *ARA&A*, 51, 393
- Curtis-Lake, E., Carniani, S., Cameron, A., et al. 2023, *Nature Astron.*, 7, 622
- Desprez, G., Martis, N. S., Asada, Y., et al. 2024, *MNRAS*, 530, 2935
- Endsley, R., Stark, D. P., Whitler, L., et al. 2023, *MNRAS*, 524, 2312
- Finkelstein, S. L., Leung, G. C. K., Bagley, M. B., et al. 2023, arXiv, 2311.04279
- Franco, M., Akins, H. B., Casey, C. M., et al. 2023, arXiv e-prints, arXiv:2308.00751
- Fujimoto, S., Arrabal Haro, P., Dickinson, M., et al. 2023, *ApJL*, 949, L25, 18 pp.
- Gao, C.-Y., López-Corredoira, M., & Wei, J.-J. 2024, *ApJ*, submitted
- Glazebrook, K., Schreiber, C., Labbé, I., et al. 2017, *Nature*, 544, 71
- Glazebrook, K., Nanayakkara, T., Jacobs, C., et al. 2023, *ApJ*, 947, L25
- Goulding, A. D., & Greene, J. E. 2022, *ApJL*, 938, L9, 8 pp.
- Guo, Q., White, S., Boylan-Kolchin, M., et al. 2011, *MNRAS*, 413, 101
- Gupta, R. 2023, *MNRAS*, 524, 3385
- Ilbert, O., Arnouts, S., McCracken, H. J., et al. 2006, *A&A*, 457, 841
- Kocevski, D. D., Onoue, M., Inayoshi, K., et al. 2023, *ApJL*, 954, L4, 17 pp.
- Labbé, I., van Dokkum, P., Nelson, E., et al. 2023, *Nature*, 616, 266
- López-Corredoira, M. 2010, *AJ*, 139, 540
- López-Corredoira, M. 2022, *Fundamental Ideas in Cosmology. Scientific, philosophical and sociological critical perspectives* (Bristol: IoP Publishing)
- López-Corredoira, M., Vazdekis, A., Gutiérrez, C. M., & Castro-Rodríguez, N. 2017, *A&A*, 600, A91, 13 pp.
- Mallory, K., Calzetti, D., & Lin, Z. 2022, *ApJ*, 933, 156
- Markov, V., Gallerani, S., Pallottini, A., et al. 2023, *A&A*, 679, A12
- McLaughlin, D. E., & van der Marel, R. P. 2005, *ApJS*, 161, 304
- Melia, F. 2020, *The Cosmic Spacetime* (Cambridge: Routledge, Taylor & Francis)
- . 2023, *MNRAS*, 521, L85
- Melia, F., & Shevchuk, A. S. H. 2012, *MNRAS*, 419, 2579
- Neeleman, M., Xavier Prochaska, J., Kanekar, N., & Rafelski, M. 2020, *Nature*, 581, 269
- Pacifici, C., Iyer, K. G., Mobasher, B., et al. 2023, *ApJ*, 944, 141
- Rocca-Volmerange, B., Hilberer, A., & Fioc, M. 2018, arXiv e-prints, arXiv:1812.04283
- Schaerer, D., Marques-Chaves, R., Barrufet, L., et al. 2022, *A&A*, 665, L4
- Schiavon, R. P., Faber, S. M., Konidaris, N., et al. 2006, *ApJ*, 651, L93
- Schreiber, C., Glazebrook, K., Nanayakkara, T., et al. 2018, *A&A*, 618, A85
- Spinrad, H., Dey, A., Stern, D., et al. 1997, *ApJ*, 484, 581
- Steinhardt, C. L., Capak, P., Masters, D., & Speagle, J. S. 2016, *ApJ*, 824, id. 21, 9 pp.
- Steinhardt, C. L., Sneppen, A., Clausen, T., et al. 2023, arXiv.org, 2305.15459
- Tremonti, C. A. 2003, PhD thesis, Johns Hopkins University, Maryland
- Vazdekis, A., & Arimoto, N. 1999, *ApJ*, 525, 144
- Vikaeus, A., Zackrisson, E., Wilkins, S., et al. 2024, *MNRAS*, 529, 1299
- Wang, F., Yang, J., Fan, X., et al. 2021, *ApJL*, 907, L1
- Weingartner, J. C., & Draine, B. T. 2001, *ApJ*, 548, 296
- Whitler, L., Endsley, R., Stark, D. P., et al. 2023, *MNRAS*, 519, 157
- Windhorst, R. A., Cohen, S. H., Jansen, R. A., et al. 2023, *AJ*, 165, 13
- Yamada, Y., Arimoto, N., Vazdekis, A., & Peletier, R. F. 2006, *ApJ*, 637, 200

Table 4

Probabilities of the discrete values of ages of the old population providing a fit of the stacked SED at rest of the 13 galaxies (corresponding to Fig. 2) using two SSPs. The P_{mlh} values are calculated through maximum likelihood. P_{Avni} are calculated using Equation (2).

t (Gyr)	χ_{red}^2	$P_{\text{mlh}}(\text{age}_{\text{old}} \leq t)$	$\frac{P_{\chi_n^2, N_{\text{dof}}(\text{age}_{\text{old}} \leq t)}}{P_{\chi_n^2, N_{\text{dof}}(\text{age}_{\text{old}} \leq 11 \text{ Gyr})}}$	$P_{\text{Avni}}(\text{age}_{\text{old}} \leq t)$
0.005	–	0	0	0
0.025	31.25	1.1×10^{-6}	3.2×10^{-5}	2.7×10^{-4}
0.10	33.25	1.1×10^{-6}	3.2×10^{-5}	2.7×10^{-4}
0.29	32.39	1.1×10^{-6}	3.2×10^{-5}	2.7×10^{-4}
0.64	27.19	1.0×10^{-5}	2.2×10^{-4}	1.8×10^{-3}
0.90	19.57	6.7×10^{-4}	6.5×10^{-3}	0.043
1.4	14.58	0.011	0.058	0.247
2.5	11.25	0.067	0.205	0.611
5.0	7.56	0.509	0.730	0.986
11.0	6.34	1	1	1

APPENDIX

A. CALCULATION OF THE ERROR BARS THROUGH A MAXIMUM LIKELIHOOD ALGORITHM

The error bars throughout this paper are calculated by identifying the portion of parameter space with a χ^2 value lower than the established numbers in χ^2 statistics (§3.1). Here we describe an alternative way of deriving them based on a Bayesian maximum likelihood approach.

We calculate the value of χ^2 for each set of parameters ($\Pi \equiv \Pi_j$; $j = 1, \dots, n_{\text{par}}$) in comparison with the data, and we choose the solution with maximum likelihood \mathcal{L} with respect to a parameter Π_i to obtain a value between x and $x + dx$, such that

$$\mathcal{L}(x < \Pi_i < x + dx) = \frac{\text{Max}[P[\text{data}|\Pi_i = x; (\Pi_j; j \neq i)]]dx}{\int d\Pi_i \text{Max}[P[\text{data}|\Pi_i; (\Pi_j; j \neq i)]]}, \quad (\text{A1})$$

where we take

$$P(\text{data}|\Pi) = \exp\left(-\frac{\chi_n^2(\text{data}|\Pi)}{2}\right). \quad (\text{A2})$$

The quantity $\chi_n^2(\text{data}|\Pi)$ is the χ^2 of the data in comparison with the model with the set of parameters Π normalizing the error bars to obtain $\chi_{\text{red, minimum}}^2 = 1$ (that is, $\chi_n^2(\text{data}|\Pi) = \frac{N_{\text{dof}}\chi^2(\Pi)}{\chi_{\text{minimum}}^2}$). This means assuming that the best fit is a reasonable fit with $\chi_{\text{red, minimum}}^2 = 1$, and we correct the under/over-estimation of error bars by multiplying them by a factor $\sqrt{\chi_{\text{red, minimum}}^2}$, the same assumption that was used in §3.1. We note that, with this normalization of χ_n , we are being more conservative, allowing a wider range of values for the parameters when $\chi_{\text{red, minimum}}^2 > 1$, which happens in most of our cases.

For our particular situation, among the seven (or six if we fix the redshift) parameters, the most interesting one to explore is the age_{old} . We carry out the calculation for the data of fluxes of the stacked SED of 13 galaxies (corresponding to Fig. 2). The probabilities for the 10 discrete values of ages we are using are given in Table 4. Interpolating from these numbers we find that: $\text{age}_{\text{old, stacked}} \geq 3.9 \text{ Gyr}$ (68%CL), and $\geq 2.1 \text{ Gyr}$ (95%CL).

B. WEIGHTED AVERAGE IN ASYMMETRICAL GAUSSIAN DISTRIBUTIONS

Here, we carry out the weighted average of $\log_{10}(\text{age}_{\text{old}})$. Assuming that the positive and negative errors are Gaussian (an asymmetrical Gaussian when the positive and negative error are different), the probability P of each galaxy to have age x is

$$P_i(x) = \frac{\sqrt{2/\pi}}{\sigma_l + \sigma_r} \times \begin{cases} \exp\left[-\frac{(x-\tau_i)^2}{2\sigma_l^2}\right] & ; \text{if } x \leq \tau_i \\ \exp\left[-\frac{(x-\tau_i)^2}{2\sigma_r^2}\right] & ; \text{if } x > \tau_i, \end{cases} \quad (\text{B1})$$

where the τ_i means the i^{th} age_{old} , and σ_l, σ_r are, respectively, the negative and positive 1σ errors. By taking the cumulative product over all distributions, we can obtain the distribution of the average age:

$$P_{\text{aver}}(x) = K \times \prod_{i=1}^n P_i(x), \quad (\text{B2})$$

where n is the number of galaxies in each redshift bin, and K is a normalization constant. Afterwards, by identifying the 0.159, 0.5, and 0.841 quantiles of the overall distribution, we obtain the lower limit, median, and upper limit of its $1\text{-}\sigma$ confidence interval; or 0.023, 0.5, and 0.977 quantiles for $2\text{-}\sigma$.

In order to take into account the possibility that the error bars do not overlap, we add a factor of correction $\sqrt{\frac{\chi^2}{N-1}}$ for the error bars.

C. SED FIT WITH *LE PHARE* PACKAGE

Le PHARE is a set of Fortran commands to compute photometric redshifts and to perform SED fitting of galaxies, QSOs or stars (Arnouts et al. 1999; Ilbert et al. 2006).⁹ We will use it in this section to show that the results obtained with our own procedure (§3.1) are compatible with those obtained with this publically available package (*le PHARE*).

We take the stacked SED at rest of the 13 galaxies (corresponding to Fig. 2), assuming that the photometric redshifts we obtained are approximately correct within their error bars. This is indeed already confirmed by comparing our results with those obtained independently by Labbé et al. (2023). And we have also seen that the stacked SED with only the four galaxies with spectroscopic redshift gives approximately the same V-shaped SED. We run the *le PHARE* to fit the best galaxy template with extinction that fits our data.

Le PHARE does not use the combination of two SSPs as we have used in §3.1. Instead, it adopts models of exponential star formation history of the type

$$F_{\text{theor.}}(\lambda_i) = \frac{L_0}{4\pi d_L(z)^2(1+z)} \times \int_0^{\text{age}} dt \left\langle \exp\left(-\frac{\text{age}-t}{\tau}\right) L_{\text{SSP}}(t, [M/H], A_V; \lambda/(1+z)) \right\rangle_T. \quad (\text{C1})$$

The stacked SED already sets $z = 0$. There are five free parameters here: the amplitude L_0 , metallicity $[M/H]$, age, τ and A_V . The templates for different values of age, τ and $[M/H]$ are taken from GISELL library with Salpeter IMF (Arnouts et al. 1999; 2002). The extinction is taken from Calzetti’s law (Calzetti et al. 2000) (§3.1).

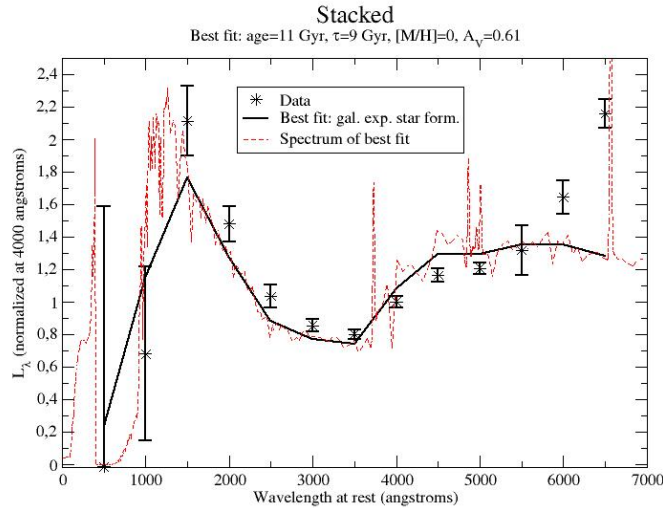


Figure 8. Best fit using *le PHARE* package with exponential star formation history ($\chi_{\text{red}}^2 = 14.99$).

The result of the best fit is shown in Fig. 8, corresponding to an age = $11.2^{+1.4}_{-1.5}$ Gyr (68% CL), $\tau = 9$ Gyr, $[M/H]=0$, $A_V = 0.61$ with a $\chi^2 = 119.9$ (hence, $\chi_{\text{red}}^2 = 14.99$). This is a worse fit than the one we obtained with two SSPs ($\chi^2 = 44.4$; $\chi_{\text{red}}^2 = 6.34$), which indicates that our model with two SSPs works much better than an exponential star formation history in V-shaped SEDs, something that had already been demonstrated by López-Corredoira et al. (2017). Nonetheless, it is remarkable that our best fit corresponds to the same age as that with two SSPs.

The best fit with an age < 0.5 Gyr is obtained for age = 64 Myr, $\tau = 0.1$ Gyr, $[M/H]=0$, $A_V = 2.43$ with a $\chi^2 = 174.7$ (hence, $\chi_{\text{red}}^2 = 21.82$). With such a very low τ , it is almost equivalent to a constant star formation ratio with an average age ~ 30 Myr, which corresponds to our fit in Fig. 4/Middle panel with one SSP of 25 Myr, a very

⁹ <http://www.cfht.hawaii.edu/~arnouts/lephare.html>

Table 5

Best fit results with two SSPs and the constraint that $\text{age}_{\text{old}} < \text{age}_{\text{Univ.}}(z)$. Errors represent the limits for which the templates of GALAXEV fit the data within 95% CL ($\equiv 2\sigma$) (within the resolution of the templates). The ages are expressed in Gyr. Redshifts of id. 13050, 28984, 35900, 39575 are fixed to their spectroscopic [S] values (<https://dawn-cph.github.io/dja/spectroscopy/nirspec/>). References for the spectroscopic redshifts: Kocevski et al. (2023): [Koc23]; Fujimoto et al. (2023): [Fuj23].

Galaxy ID	z	$\log_{10}[\text{age}_{\text{old}}]$	$\log_{10}[\text{age}_{\text{young}}]$	A_2	$[M/H]$	A_V	χ_{red}^2
2859	$10.48^{+1.32}_{-5.48}$	$-0.54^{+0.49}_{-1.06}$	$-2.30^{+2.11}_{-0}$	$0.04^{+0.68}_{-0.04}$	$+0.4^{+0}_{-0.8}$	$0.67^{+2.33}_{-0.67}$	9.20
7274	$10.47^{+1.33}_{-5.47}$	$-0.54^{+0.49}_{-1.06}$	$-2.30^{+2.11}_{-0}$	$0.05^{+0.55}_{-0.05}$	$+0.4^{+0}_{-0.8}$	0^{+2}_{-0}	91.62
11184	$7.18^{+0.47}_{-0.39}$	$-0.54^{+0.34}_{-0.46}$	$-1.00^{+0.29}_{-1.30}$	$0.48^{+0.16}_{-0.47}$	$0^{+0}_{-0.4}$	$0^{+0.75}_{-0}$	11.62
13050	5.62 [Koc23]	$-1.60^{+0.22}_{-0.56}$	$-2.30^{+2.11}_{-0.00}$	$0^{+0.55}_{-0}$	$+0.4^{+0}_{-0.8}$	$4.26^{+0.84}_{-3.26}$	8.31
14924	$9.83^{+0.53}_{-0.43}$	$-0.54^{+0.21}_{-0.17}$	$-2.30^{+1.30}_{-0}$	$0.04^{+0.26}_{-0.04}$	$0^{+0}_{-0.4}$	$0.23^{+1.27}_{-0.23}$	5.71
16624	$10.20^{+0.88}_{-0.85}$	$-0.54^{+0.21}_{-0.46}$	$-2.30^{+1.30}_{-0}$	$0.08^{+0.49}_{-0.07}$	$0^{+0}_{-0.4}$	$0.11^{+0.89}_{-0.11}$	9.06
21834	$10.17^{+1.03}_{-0.53}$	$-0.54^{+0.21}_{-0.46}$	$-2.30^{+1.30}_{-0}$	$0.04^{+0.44}_{-0.04}$	$+0.4^{+0}_{-0.8}$	$0.04^{+1.96}_{-0.04}$	1.46
25666	$7.59^{+2.41}_{-2.59}$	$-0.19^{+0.15}_{-1.41}$	$-2.30^{+2.11}_{-0}$	$0.20^{+0.40}_{-0.20}$	$+0.4^{+0}_{-0.8}$	$0.53^{+1.47}_{-0.53}$	36.15
28984	7.09 [S]	$-0.19^{+0.08}_{-1.41}$	$-2.30^{+1.76}_{-0}$	$0.33^{+0.32}_{-0.33}$	$+0.4^{+0}_{-0.8}$	$1.24^{+0.86}_{-1.24}$	17.44
35300	7.77 [Fuj23]	$-0.19^{+0.08}_{-1.41}$	$-2.30^{+1.76}_{-0.00}$	$0.36^{+0.24}_{-0.35}$	$+0.4^{+0}_{-0.8}$	$2.02^{+0.98}_{-2.02}$	4.70
37888	$7.24^{+2.76}_{-2.24}$	$-0.19^{+0.15}_{-1.41}$	$-2.30^{+2.11}_{-0}$	$0.26^{+0.34}_{-0.26}$	$+0.4^{+0}_{-0.8}$	$0.41^{+1.59}_{-0.41}$	9.43
38094	$8.10^{+0.62}_{-2.10}$	$-0.54^{+1.58}_{-0.46}$	$-2.30^{+2.11}_{-0}$	$0.02^{+0.58}_{-0.02}$	$0^{+0}_{-0.4}$	$0.42^{+1.58}_{-0.42}$	142.92
39575	7.99 [Fuj23]	$-0.54^{+0.21}_{-1.06}$	$-2.30^{+1.30}_{-0}$	$0.56^{+0.28}_{-0.55}$	-0.4 ± 0	$1.44^{+0.66}_{-1.44}$	4.21

high extinction of $A_V = 2.48$ and $\chi^2 = 170.1$. This is a much worse fit because such a high extinction erases the Lyman- α peak.

le PHARE also allows for the possibility of fitting a QSO among the different templates available with a different continuum power index α and equivalent width (EW measured for lines Ly α +NV), without extinction. The best fit corresponds to $\chi^2 = 155.3$ for $\alpha = -1.25$, $EW = 84 \text{ \AA}$. However, the template of the best fit corresponding to synthetic spectra provides fluxes only for $\lambda \geq 600 \text{ \AA}$, setting zero flux for lower wavelengths, thus giving a false agreement with the point of the bin at 500 \AA and considerably reducing the χ^2 with respect to its value when an extrapolation of the template to shorter wavelengths is introduced. Moreover, the extrapolation of Calzetti's law to wavelengths below 1200 \AA is not appropriate. This is critical, because the non-detection of the galaxies in the HST filter F435W and the huge dropoff at wavelengths shorter than Lyman- α is a clear indication of the incompatibility with any QSO SED. Furthermore, it fails to reproduce the area around the Balmer break, since the QSO yields blue colors at all wavelengths. A combination of QSO+galaxy might improve the fit, but *le PHARE* does not allow for the possibility of such fits. We have carried out this kind of combination of QSO with 2-SSPs and we have seen that adding a QSO component does not improve the fit (see §3.4).

D. SED FITS WITH THE AGE OF GALAXIES RESTRICTED TO BE YOUNGER THAN THAT OF THE UNIVERSE

In Table 5, we show the results of the best fit with 2SSP, following the method described in §3.1, but with the extra constraint that $\text{age}_{\text{old}} < \text{age}_{\text{Univ.}}(z)$, where $\text{age}_{\text{Univ.}}(z)$ is the age of the Universe at redshift z predicted by the standard model. As we can see, the values of χ_{red}^2 are much higher than those shown in Table 1, based on calculations without this constraint: on average, χ_{red}^2 is 2.2 times larger in Table 5 than in Table 1. The much worse fits when the galaxies' age is constrained to be less than that of the Universe can also be seen in the optimization of the stacked SED: Left panel of Fig. 4 compared with Fig. 2.

The fact that Labbé et al. (2023) (see also Barro et al. (2024) for similar SED fittings of the JWST galaxies) are able to fit these 13 galaxies with ages younger than that of the Universe is due to their assumption of a lower, or no, extinction for the young population, which is—in our view—inappropriate because the dust extinction (if any) should be applied to the whole stellar population, especially the youngest component that produces the Far-UV break, given that the dust is more abundant in young populations (Mallory et al. 2022). At a minimum, extinction in the young population cannot be lower than the extinction in the old population.